arXiv:cond-mat/0501728v3 [cond-mat.supr-con] 20 Jul 2005

Conventional character of the BCS-BEC cross-over in ultra-cold gases of ^{40}K

Marzena H. Szymańska,[1] Krzysztof Góral,[2] Thorsten Köhler,[2] and Keith Burnett[2]
[1]*Cavendish Laboratory, Department of Physics, University of Cambridge, Madingley Road, Cambridge CB3 OHE, UK*
[2]*Clarendon Laboratory, Department of Physics, University of Oxford, Parks Road, Oxford, OX1 3PU, UK*

(Dated: February 2, 2008)

We use the standard fermionic and boson-fermion Hamiltonians to study the BCS-BEC cross-over near the 202 G resonance in a two-component mixture of fermionic ^{40}K atoms employed in the experiment of C.A. Regal *et al.* [Phys. Rev. Lett. **92**, 040403 (2004)]. Our mean-field analysis of many-body equilibrium quantities shows virtually no differences between the predictions of the two approaches, provided they are both implemented in a manner that properly includes the effect of the highest excited bound state of the background scattering potential, rather than just the magnetic-field dependence of the scattering length. Consequently, we rule out the macroscopic occupation of the molecular field as a mechanism behind the fermionic pair condensation and show that the BCS-BEC cross-over in ultra-cold ^{40}K gases can be analysed and understood on the same basis as in the conventional systems of solid state physics.

PACS numbers: 03.75.Ss, 03.75.Nt, 34.50.-s

I. INTRODUCTION

Dilute vapours of fermionic atoms have recently attracted considerable attention as systems for studying the cross-over between Bardeen-Cooper-Schrieffer (BCS) pairing and Bose-Einstein condensation (BEC) of self-bound pairs of particles [1, 2, 3, 4, 5]. The experimental techniques underlying these studies all take advantage of the unique possibility of controlling the inter-atomic interactions via magnetically tunable Feshbach resonances. Observations of both molecular BEC [6, 7, 8] and condensation of unbound fermionic pairs [9, 10] in gases containing incoherent mixtures of two different spin components have recently been reported. The properties of both phases have been studied in several recent experiments [11, 12, 13, 14, 15, 16].

The principal question of whether the BCS-BEC cross-over in ultra-cold atomic gases can be analysed and understood on the same basis as in the traditional systems of solid state physics [1, 2, 3, 4, 5] is, however, a matter of continuing controversy. This controversy dates back to the first predictions of a superfluid phase transition in dilute Fermi gases using Feshbach resonances [17, 18], suggesting a new type of pair condensation based on a macroscopic occupation of the Feshbach resonance level. The concept underlying this idea of resonance superfluidity [17, 18] was motivated by the use of an effective boson-fermion Hamiltonian [19, 20], which treats pairs of atoms in the resonance state configuration in terms of single structureless Bose particles, often referred to as “molecules”. The studies of Refs. [21, 22] have clearly shown, however, that the experimentally relevant highest excited vibrational multi-channel molecular bound state (the Feshbach molecule) is, in general, significantly different from the Feshbach resonance level (belonging to the closed scattering channel) and requires an explicit description in terms of a composite two-body system.

In this paper we demonstrate that the thermal equilibrium physical quantities, relevant to recent experiments on the BCS-BEC cross-over in cold gases using broad Feshbach resonances of ^{40}K and ^{6}Li, can all be described by the usual fermionic Hamiltonian for a gas with two spin components and separable binary interactions [3, 4, 23]. Consequently, we rule out the macroscopic occupation of the Feshbach resonance level as a mechanism behind the superfluid pairing in these systems. To this end, we compare predictions obtained from both the standard fermionic and boson-fermion Hamiltonians adjusted in such a way that they both recover the low energy binary collision physics over a wide range of magnetic field strengths, beyond the regime of universality. These adjustments are performed on the basis of a two-channel description of the resonance enhanced binary scattering involving the entrance channel of the spatially separated atoms and a closed channel strongly coupled to it via the Feshbach resonance level. Our approach [24] depends on five measurable parameters of a Feshbach resonance and is applicable to both narrow (closed channel dominated) and broad (entrance channel dominated) resonances.

Throughout this paper we shall discuss a balanced mixture of ^{40}K atoms prepared in the $(f = 9/2, m_f = -9/2)$ and $(f = 9/2, m_f = -7/2)$ Zeeman states (cf., e.g., Ref. [9]). We consider magnetic field strengths in the vicinity of the 202 G (1 G = 10^{-4} T) zero-energy resonance (singularity of the scattering length). This ^{40}K Feshbach resonance is particularly well suited to demonstrate the wide range of applicability of our approach, as its width is in between those of the experimentally relevant extremely narrow (closed channel dominated) and broad (entrance channel dominated) resonances of ^{6}Li at about 543 [25] and 830 G [7, 8, 12, 13], respectively. While the general differences between closed and entrance channel dominated Feshbach resonances were discussed in Ref. [26], the very different universal regimes of magnetic field strengths of ^{6}Li resonances and their potential relevance to the BCS-BEC cross-over were the subject of the recent studies of Ref. [27].

The paper is organised as follows: In Section II we describe the two-channel approach to the resonance enhanced low energy binary scattering observables and introduce the five relevant physical parameters for the 202 G zero-energy resonance of ^{40}K. These two-body considerations reveal that the admixture of the Feshbach resonance level to the experimentally relevant bound Feshbach molecule never exceeds 8% over the entire range of magnetic fields relevant to the experiment of Ref. [9]. Its maximum value is reached at about 7.2 G below the position of $B_0 = 202.1$ G [9] of the zero-energy resonance. These results are in agreement with exact coupled channels calculations [28] from which the two-channel approach was originally derived in Ref. [24]. Our analysis reveals that a proper description of the admixture of the resonance level to the multi-channel bound and scattering states requires a two-channel approach to explicitly account for the entrance channel background scattering potential including its highest excited vibrational state. Given the small admixture of the resonance level to the Feshbach molecule, we then determine an accurate separable single channel potential, which is suitable for the standard fermionic many-body Hamiltonian. This potential is adjusted in such a way that it accurately describes not only the magnetic field dependence of the scattering length but also the binding energy of the Feshbach molecule.

In Section III we discuss the implications of the nature of the resonance enhanced binary collision physics for the potentials and parameters of both the standard fermionic and boson-fermion Hamiltonians. The procedure of adjusting these effective Hamiltonians involves the identification of the two-body resonance level with the structureless Bose particles of the boson-fermion approach. Its background scattering potential and inter-channel coupling parameters are then determined in such a way that they exactly reproduce the predictions of the two-channel approach of Ref. [24] when applied to a pair of atoms.

Section IV briefly summarises the mean-field approach we have used to determine the thermodynamic quantities for both the standard fermionic and the boson-fermion Hamiltonians. In Section V we then apply this mean-field approach to the BCS-BEC cross-over in a cold gas of ^{40}K with a particular emphasis on the experimental conditions of Ref. [9]. We show that, as expected from our two-body analysis, the standard fermionic and boson-fermion Hamiltonians lead to virtually the same predictions about the equilibrium physics. In particular, our analysis supports the picture of a smooth cross-over of the pair size in the entrance channel characterised by features similar to those of traditional superconductivity [1, 2, 3, 4, 5] and exciton and polariton [1, 29, 30, 31] condensates. We therefore conclude that the occupation of the Feshbach resonance level is irrelevant to the nature of fermionic superfluidity in a cold ^{40}K gas, in contrast to the findings of Refs. [32, 33]. We predict the position of the zero of the chemical potential (cross-over point) at 0.32 G below the zero-energy resonance. We have, furthermore, analysed the experimental pairwise projection technique of Ref. [9] by calculating the overlap between the fermionic pairs produced on the high field side of the ^{40}K resonance and the bound Feshbach molecule on its low field side. Our results indicate that fermionic pair condensation phenomena should become invisible once the gas is prepared at magnetic field strengths further than about 0.5 G above the resonance position. Finally, Section VI summarises our main conclusions.

II. MAGNETICALLY TUNABLE INTER-ATOMIC INTERACTIONS

At the low collision energies characteristic of cold dilute gases the binary scattering physics can be described by a single parameter of the inter-atomic potential, the s-wave scattering length a. The experimental technique of Feshbach resonances takes advantage of the Zeeman effect in the atomic energy levels to widely tune the scattering length using magnetic fields. In the experiments of Ref. [9] the gas was prepared as a balanced, incoherent mixture of the lowest energetic $(f = 9/2, m_f = -9/2)$ and $(f = 9/2, m_f = -7/2)$ Zeeman levels at magnetic field strengths on the order of 200 G. Only pairs of unlike fermions in different Zeeman levels can interact via s waves which dominate cold collisions (in the absence of resonant phenomena associated with higher partial waves). Throughout this paper we shall denote the asymptotic s-wave binary scattering channel of a pair of these unlike ^{40}K atoms as the entrance channel, while its associated interaction potential V_{bg} will be referred to as the background scattering potential. As the m_f degeneracy of the Zeeman levels is removed by a homogeneous magnetic field of strength B, the potentials associated with the different scattering channels can be shifted with respect to each other. The typically weak inter-channel coupling becomes significantly enhanced when the magnetic field dependent energy $E_{\mathrm{res}}(B)$ (see Fig. 1) of a closed channel vibrational state ϕ_{res} (the Feshbach resonance level) is tuned in the vicinity of the dissociation threshold of the entrance channel. Since this threshold coincides with the zero of collision energy (zero of energy in Fig. 1), its virtual degeneracy with $E_{\mathrm{res}}(B)$ leads to a resonance enhancement of the cold inter-atomic collisions in terms of a zero-energy resonance in the entrance channel, i.e. a singularity of the scattering length at the magnetic field strength B_0 described by the formula:

$$a(B) = a_{\mathrm{bg}}\left(1 - \frac{\Delta B}{B - B_0}\right). \tag{1}$$

The parameters a_{bg} and ΔB are usually referred to as the background scattering length and the resonance width, respectively.

The magnetic tuning of the energy of the Feshbach resonance level distorts not only the scattering continuum but also the bound multi-channel molecular energy levels. As illustrated in Fig. 1, the position $B_0 = 202.1$ G of the zero-energy resonance, i.e. the magnetic field strength at which the scattering length has its singularity, coincides with the zero of the binding energy $E_{\mathrm{b}}(B)$ of the highest excited multi-channel vibrational state. This Feshbach molecular state $\phi_{\mathrm{b}}(B)$ persists on the low field side of the 202 G zero-energy resonance of ^{40}K where $a(B)$ is positive, while it ceases to exist on the high field side of negative scattering lengths. We note that the measurable resonance position B_0 is shifted with respect to the magnetic field strength B_{res} (see Fig. 1) at which the energy $E_{\mathrm{res}}(B)$ crosses the dissociation threshold of the entrance channel. In fact, the multi-channel bound state $\phi_{\mathrm{b}}(B)$ and the meta-stable Feshbach resonance level are, in general, rather distinct objects, in particular, when the inter-channel coupling

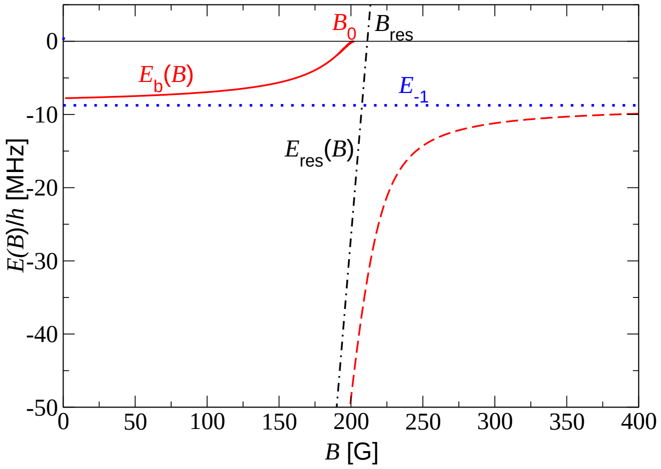

FIG. 1: (Color online) Binding energies of the highest excited multi-channel vibrational molecular bound states (solid and dashed curves), associated with a pair of unlike ^{40}K atoms in the asymptotic $(f=9/2, m_f=-9/2)$ and $(f=9/2, m_f=-7/2)$ Zeeman states, versus the magnetic field strength B. The Feshbach molecular state $\phi_{\rm b}(B)$ and its energy $E_{\rm b}(B)$ emerge at the position of the zero-energy resonance B_0. The linearly varying energy $E_{\rm res}(B)$ of the Feshbach resonance level $\phi_{\rm res}$ and the energy E_{-1} of the highest excited vibrational state of the background scattering potential are indicated by the dot-dashed and dotted lines, respectively. We note that the measurable resonance position B_0 is significantly shifted with respect to the magnetic field strength $B_{\rm res}$ at which the closed-channel resonance state energy crosses the dissociation threshold of the entrance channel. Here and throughout this paper, we have chosen the zero of the energy, at each magnetic field strength B, as the sum of the Zeeman energies of a pair of unlike fermions.

is strong.

A. Two-channel approach

To accurately describe the resonance enhancement of the binary collisions as well as the properties of the Feshbach molecule of a pair of unlike ^{40}K fermions, we employ the approach of Ref. [24], which explicitly includes the entrance channel and its strong coupling to a closed channel via the Feshbach resonance level. According to the effective treatment of Ref. [24], the general form of a two-channel Hamiltonian matrix

$$H_{\rm 2B-2ch} = \begin{pmatrix} -\frac{\hbar^2}{m}\nabla^2 + V_{\rm bg} & W \\ W & -\frac{\hbar^2}{m}\nabla^2 + V_{\rm cl}(B) \end{pmatrix} \tag{2}$$

depends on five physical parameters in addition to the atomic mass m: The background scattering potential $V_{\rm bg}$ of the entrance channel is characterised by the energy E_{-1} of its highest excited vibrational state and the background scattering length $a_{\rm bg}$ [34], while the closed channel potential $V_{\rm cl}(B)$ can be effectively described by the constant difference $dE_{\rm res}/dB$ between the magnetic moments of the Feshbach resonance level and a pair of asymptotically separated ^{40}K fermions in the $(f=9/2, m_f=-9/2)$ and $(f=9/2, m_f=-7/2)$ Zeeman states. The inter-channel coupling is accounted for by the off-diagonal potential W whose strength and range parameter are determined by the resonance width ΔB and the shift $B_0-B_{\rm res}$ (see Fig. 1).

At the low relative momenta and associated large de Broglie wavelengths characteristic for cold gases, the details of the microscopic binary interaction potentials are not resolved. Reference [24], therefore, suggests a convenient effective potential matrix that recovers all the relevant low energy physical observables of the exact microscopic binary interaction.

1. Adjustment of the background scattering potential

Following the treatment of Ref. [24], we use the following separable form of the background scattering potential:

$$V_{\rm bg} = |\chi_{\rm bg}\rangle\xi_{\rm bg}\langle\chi_{\rm bg}|\,. \tag{3}$$

For the form factor $|\chi_{\rm bg}\rangle$ we choose the Gaussian *ansatz*:

$$\langle\mathbf{p}|\chi_{\rm bg}\rangle = \chi_{\rm bg}(p) = \frac{\exp\left(-\frac{p^2\sigma_{\rm bg}^2}{2\hbar^2}\right)}{(2\pi\hbar)^{3/2}}\,. \tag{4}$$

Here $|\mathbf{p}\rangle$ is a plane wave momentum state, normalised as $\exp(i\mathbf{p}\cdot\mathbf{r}/\hbar)/(2\pi\hbar)^{3/2}$. The amplitude $\xi_{\rm bg}$ and the range parameter $\sigma_{\rm bg}$ can be adjusted in such a way that $V_{\rm bg}$ exactly recovers $a_{\rm bg}$ and E_{-1} as follows: The first condition for the adjustments is given by the relationship between the background scattering length and the zero-energy T matrix associated with the background scattering potential. The exact analytic expression for this T matrix given in Ref. [24] yields:

$$a_{\rm bg} = \frac{\frac{m}{4\pi\hbar^2}\xi_{\rm bg}}{1+\frac{m}{4\pi^{3/2}\hbar^2\sigma_{\rm bg}}\xi_{\rm bg}}\,. \tag{5}$$

The second condition is equivalent to the stationary Schrödinger equation for a bound state of the separable potential and reads [24]:

$$\frac{m}{4\pi^{3/2}\hbar^2\sigma_{\rm bg}}\xi_{\rm bg}\left[\sqrt{\pi}xe^{x^2}{\rm erfc}(x)-1\right] = 1. \tag{6}$$

Here ${\rm erfc}(x) = \frac{2}{\sqrt{\pi}}\int_x^\infty e^{-u^2}du$ is the complementary error function (sometimes referred to as the Hechenblaikner function) with the argument $x=\sqrt{m|E_{-1}|}\sigma_{\rm bg}/\hbar$. We note that the positivity of the background scattering length $a_{\rm bg} = 174\,a_{\rm Bohr}$ [35] ($a_{\rm Bohr} = 0.052918$ nm is the Bohr radius) guarantees the existence of a single bound state of the separable potential $V_{\rm bg}$ for two unlike ^{40}K fermions. Equations (5) and (6) then simultaneously determine the parameters $\sigma_{\rm bg}$ and $\xi_{\rm bg}$.

2. Single-resonance approximation in the closed channel

In most of the experimentally relevant cases the entrance channel is strongly coupled only to a single closed channel vibrational state, i.e. the Feshbach resonance level $\phi_{\rm res}$. It is therefore usually sufficient to restrict the spatial configuration of a closed channel atom pair to $\phi_{\rm res}(r)$, where r is the inter-atomic separation. To this end Ref. [24] introduces the single-resonance approximation (referred to as the pole approximation in Ref. [24]) which consists in replacing the diagonal closed channel part of the general Hamiltonian matrix (2) by the one dimensional projection onto the resonance level, i.e.

$$-\hbar^2\nabla^2/m + V_{\rm cl}(B) \to |\phi_{\rm res}\rangle E_{\rm res}(B)\langle\phi_{\rm res}|. \tag{7}$$

The resonance energy varies virtually linearly with the magnetic field strength B and can therefore be described by the first term of the power series expansion about its zero at $B_{\rm res}$, which reads:

$$E_{\rm res}(B) = \frac{dE_{\rm res}}{dB}(B - B_{\rm res})\,. \tag{8}$$

Here $dE_{\rm res}/dB$ is the magnetic moment of the resonance level with respect to the sum of magnetic moments of a pair of asymptotically separated unlike fermions. It can be obtained either from measurements of the binding energies of the Feshbach molecule away from the zero-energy resonance or from exact coupled channels calculations using microscopic interactions.

3. *Inter-channel coupling*

In accordance with the preceding single-resonance approximation to the closed channel Hamiltonian the inter-channel coupling is determined by the product $W|\phi_{\rm res}\rangle$ [24]. We represent this product in terms of an amplitude ζ and a wave function $|\chi\rangle$, i.e.

$$W|\phi_{\rm res}\rangle = |\chi\rangle\zeta. \tag{9}$$

The wave function $|\chi\rangle$ accounts for the spatial variation of the inter-channel coupling in terms of a range parameter σ. We choose a Gaussian *ansatz* which, in the convenient momentum space representation, is given by:

$$\langle\mathbf{p}|\chi\rangle = \chi(p) = \frac{\exp\left(-\frac{p^2\sigma^2}{2\hbar^2}\right)}{(2\pi\hbar)^{3/2}}\,. \tag{10}$$

Given that the range parameter $\sigma_{\rm bg}$ of the background scattering potential has been determined using the procedure from above, the parameters ζ and σ can be adjusted in such a way that they exactly recover the width ΔB of the zero-energy resonance as well as its shift $B_0 - B_{\rm res}$ (see Fig. 1). Following the procedure of Ref. [24], the two conditions for the simultaneous adjustment of ζ and σ are given by the exact expressions

$$\Delta B = \frac{m\zeta^2}{4\pi\hbar^2 a_{\rm bg}(dE_{\rm res}/dB)}\left(1 - \frac{a_{\rm bg}}{\sqrt{\pi}\,\overline{\sigma}}\right)^2 \tag{11}$$

for the resonance width, and

$$B_0 - B_{\rm res} = (\Delta B)\frac{a_{\rm bg}}{\sqrt{\pi}\sigma}\,\frac{1 - \frac{a_{\rm bg}}{\sqrt{\pi}\sigma}\left(\frac{\sigma}{\overline{\sigma}}\right)^2}{\left(1 - \frac{a_{\rm bg}}{\sqrt{\pi}\sigma}\frac{\sigma}{\overline{\sigma}}\right)^2} \tag{12}$$

for the associated shift. Here we have introduced the mean range parameter:

$$\overline{\sigma} = \sqrt{\frac{1}{2}\left(\sigma^2 + \sigma_{\rm bg}^2\right)}\,. \tag{13}$$

While ΔB is usually known from measurements of the magnetic field dependence of the scattering length $a(B)$ (cf. Ref. [6]), the precise value of $B_0 - B_{\rm res}$ can not be easily deduced from experimental data. Reference [24] therefore suggests an analytic treatment, based on ideas of multi-channel quantum defect theory [36], to determine the resonance shift. This treatment relates $B_0 - B_{\rm res}$ to the van der Waals dispersion coefficient C_6 in terms of the mean scattering length [37]:

$$\overline{a} = \frac{1}{\sqrt{2}}\frac{\Gamma(3/4)}{\Gamma(5/4)}\frac{1}{2}\left(\frac{mC_6}{\hbar^2}\right)^{1/4}. \tag{14}$$

Here Γ is the gamma function. The van der Waals dispersion coefficient characterises the (non-retarded) asymptotic behaviour $V_{\rm bg}(r) \underset{r\to\infty}{\sim} -C_6/r^6$ of the exact microscopic background scattering potential at large inter-atomic distances r and can be deduced from experimental observations [38]. Following the ideas of Ref. [36], the magnitude of $B_0 - B_{\rm res}$ is accurately determined by the formula:

$$B_0 - B_{\rm res} = (\Delta B)\frac{\frac{a_{\rm bg}}{\overline{a}}\left(1 - \frac{a_{\rm bg}}{\overline{a}}\right)}{1 + \left(1 - \frac{a_{\rm bg}}{\overline{a}}\right)^2}. \tag{15}$$

The procedure for the determination of the inter-channel coupling parameters ζ and σ thus consists in calculating the resonance shift using Eq. (15) and then simultaneously solving Eqs. (11) and (12).

4. *Molecular bound states*

The two-channel Hamiltonian of our approach of Ref. [24] can support two bound states. Their wave functions associated with the entrance- and closed-channel components have the following general form:

$$\begin{pmatrix} \phi_{\rm b}^{\rm bg} \\ \phi_{\rm b}^{\rm cl} \end{pmatrix} = \frac{1}{\mathcal{N}_{\rm b}}\begin{pmatrix} G_{\rm bg}(E_{\rm b})W\phi_{\rm res} \\ \phi_{\rm res} \end{pmatrix}. \tag{16}$$

Here $G_{\rm bg}(E_{\rm b})$ is the energy-dependent Green's function associated with the entrance channel, whose explicit expression reads

$$G_{\rm bg}(E_{\rm b}) = \left[E_{\rm b} - \left(-\frac{\hbar^2}{m}\nabla^2 + V_{\rm bg}\right)\right]^{-1}, \tag{17}$$

while the normalisation constant $\mathcal{N}_{\rm b}$ is given by the formula

$$\mathcal{N}_{\rm b} = \sqrt{1 + \langle\phi_{\rm res}|W\left[G_{\rm bg}(E_{\rm b})\right]^2 W|\phi_{\rm res}\rangle}\,. \tag{18}$$

The energies $E_{\rm b}$ associated with the two-channel bound states in the single resonance approximation are determined by the following condition:

$$E_{\rm b} = E_{\rm res}(B) + \langle\phi_{\rm res}|WG_{\rm bg}(E_{\rm b})W|\phi_{\rm res}\rangle\,. \tag{19}$$

The energies of the Feshbach molecular state and of the second more tightly bound two-channel state of ^{40}K are indicated in Fig. 1 by the solid and dashed curves, respectively.

5. *Parameters for a pair of unlike ^{40}K fermions*

For the experiment of Ref. [9], which uses a balanced incoherent mixture of ^{40}K atoms in the $(f = 9/2, m_f = -9/2)$ and $(f = 9/2, m_f = -7/2)$ Zeeman states at magnetic field strengths in the vicinity of the 202 G resonance, the physical parameters are given by: $a_{\mathrm{bg}} = 174\, a_{\mathrm{Bohr}}$ [35], $E_{-1} = -h \times 8.75$ MHz [28], $\Delta B = 7.8$ G [6], $B_0 - B_{\mathrm{res}} = -9.274$ G, and $dE_{\mathrm{res}}/dB = 1.679\, \mu_{\mathrm{Bohr}}$ ($\mu_{\mathrm{Bohr}} = 9.27400899 \times 10^{-28}$ J/G is the Bohr magneton). We have obtained the resonance shift $B_0 - B_{\mathrm{res}}$ from Eq. (15) using $C_6 = 3897$ a.u. [38] (1 a.u.=0.095734×10^{-78}J m^6) and the resonance slope dE_{res}/dB has been extracted from exact coupled channels calculations of the binding energy of the Feshbach molecule [28]. From these physical quantities we have determined the following parameters of the two-channel Hamiltonian: $m\xi_{\mathrm{bg}}/(4\pi\hbar^2) = -244.852\, a_{\mathrm{Bohr}}$, $\sigma_{\mathrm{bg}} = 57.387\, a_{\mathrm{Bohr}}$, $\sigma = 33.123\, a_{\mathrm{Bohr}}$, and $m\zeta^2/(4\pi\hbar^2\sigma) = h \times 80.272$ MHz. Figure 1 shows the binding energies of the multi-channel vibrational states predicted by the two-channel Hamiltonian of Eq. (2) using the parameters listed above. We note that the two-channel approach also exactly recovers the magnetic field dependence of the scattering length $a(B)$ described by Eq. (1).

B. Single-channel approach

As the magnetic field strength approaches the position B_0 of the zero-energy resonance from the positive scattering length side, the admixture of the resonance level ϕ_{res} to the physically relevant Feshbach molecular state $\phi_{\mathrm{b}}(B)$ vanishes [22, 26]. In this universal regime of magnetic field strengths it is always possible to introduce an effective single-channel Hamiltonian [21, 24, 26], which accurately recovers the resonance enhancement of the scattering as well as the universal binding energy

$$E_{\mathrm{b}} \underset{a\to+\infty}{\sim} -\frac{\hbar^2}{ma^2} \tag{20}$$

of the Feshbach molecule. The studies presented in Refs. [21, 26] have shown, however, that the range of validity of such a single-channel approach can be significantly extended by properly adjusting the binary potential of the effective Hamiltonian, provided that the resonance is broad and entrance channel dominated [26]. We shall show below that the 202 G resonance of ^{40}K fulfils all requirements for an accurate treatment of the binary low energy bound and continuum spectrum in terms of just a single asymptotic scattering channel.

The single-channel approach of Refs. [21, 24, 26] effectively describes the resonance enhancement of the low energy scattering as a perturbation of the background scattering potential. Following this approach, we replace the parameter ξ_{bg} in Eq. (3) by a magnetic field dependent amplitude $\xi_{\mathrm{eff-1ch}}(B)$ and insert the associated effective single-channel potential

$$V_{\mathrm{eff-1ch}}(B) = |\chi_{\mathrm{bg}}\rangle \xi_{\mathrm{eff-1ch}}(B) \langle\chi_{\mathrm{bg}}| \tag{21}$$

into the general form of a single-channel Hamiltonian

$$H_{\mathrm{2B-1ch}} = -\frac{\hbar^2}{m}\nabla^2 + V_{\mathrm{eff-1ch}}(B)\,. \tag{22}$$

In this treatment the range parameter σ_{bg} retains the same value as in the two-channel approach, while the amplitude $\xi_{\mathrm{eff-1ch}}(B)$ is adjusted in such a way that the effective potential recovers, at each value of the magnetic field, the scattering length $a(B)$ of Eq. (1). This adjustment can be performed in complete analogy to the determination of ξ_{bg} in the two-channel approach of Ref. [24]. The counterpart of Eq. (5) for the determination of $\xi_{\mathrm{eff-1ch}}(B)$ leads to the relationship:

$$\xi_{\mathrm{eff-1ch}}(B) = \frac{4\pi\hbar^2 a(B)/m}{1 - a(B)/(\sqrt{\pi}\sigma_{\mathrm{bg}})}\,. \tag{23}$$

We note that despite the divergence of the scattering length $a(B)$ at resonance the amplitude of the effective single-channel potential $\xi_{\mathrm{eff-1ch}}(B)$ remains a smooth function of the magnetic field strength B. The single-channel approach not only recovers the exact magnetic field dependence of the scattering length, by identifying $a(B)$ in Eq. (23) with Eq. (1), but it also leads to the exact asymptotic limit E_{-1} of the binding energy $E_{\mathrm{b}}(B)$ away from the resonance (see Fig. 1), by using the same form factor $|\chi_{\mathrm{bg}}\rangle$ as the separable background scattering potential of Eq. (3).

Figure 2 compares the binding energy $E_{\mathrm{b}}(B)$ of the Feshbach molecule, as obtained from the two-channel approach of Ref. [24], with the predictions of the effective single-channel approach, as well as analytic estimates. These estimates are based on Eq. (20) and on the formula

$$E_{\mathrm{b}} \approx -\frac{\hbar^2}{m(a-\bar{a})^2}, \tag{24}$$

which follows from the treatment of Ref. [37] and accounts for the non-retarded van der Waals tail $V_{\mathrm{bg}}(r) \underset{r\to\infty}{\sim} -C_6/r^6$ of the background scattering potential, in terms of the mean scattering length $\bar{a}$ of Eq. (14), in addition to the magnetic field dependence of the scattering length $a(B)$. As the magnetic field strength B approaches the position B_0 of the zero-energy resonance from below, all predictions coincide. In this universal regime of magnetic field strengths the scattering length very much exceeds all the other length scales set by the binary interactions and completely determines the magnitude of the binding energy. Further away from the resonance the quality of the universal estimate of Eq. (20) deteriorates, while Eq. (24) provides a good approximation of $E_{\mathrm{b}}(B)$ over the entire range of magnetic field strengths shown in Fig. 2. The full predictions of the two- and single-channel approaches are virtually indistinguishable. This agreement suggests that the admixture of the resonance level ϕ_{res} to the Feshbach molecule remains small also outside the universal regime of magnetic

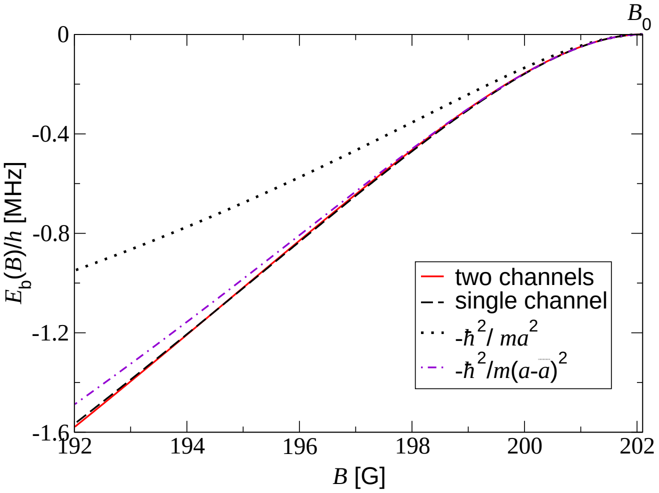

FIG. 2: (Color online) Binding energy $E_{\mathrm{b}}(B)$ of the Feshbach molecular bound state $\phi_{\mathrm{b}}(B)$ associated with a pair of unlike ^{40}K atoms in the asymptotic $(f = 9/2, m_f = -9/2)$ and $(f = 9/2, m_f = -7/2)$ Zeeman states versus the magnetic field strength B. The figure shows a comparison between the results of the two-channel approach (solid curve), the effective single-channel approach (dashed curve), and analytic estimates of the binding energy (dotted and dot-dashed curves). While the dotted curve refers to the universal estimate of Eq. (20), just depending on the scattering length $a(B)$, the dot-dashed curve also accounts for the non-retarded van der Waals interaction $-C_6/r^6$ of the background scattering potential, at asymptotically large interatomic distances r, in terms of the mean scattering length $\bar{a}$ [21, 37] via Eq. (24).

field strengths, i.e. the 202 G resonance of ^{40}K is entrance channel dominated. In fact, we shall show in Section V that the closed-channel admixture to the bound state wave function $\phi_{\mathrm{b}}(B)$ never exceeds about 8% and reaches its maximum at about 7.2 G below the position $B_0 = 202.1\,\mathrm{G}$ of the zero-energy resonance.

III. MANY-BODY HAMILTONIANS

A. The microscopic Hamiltonian

Having established the microscopic parameters of the interatomic interactions, which properly describe the experimentally relevant part of the two-body energy spectrum, we shall now discuss the many-body Hamiltonians that we use in our studies of the BCS-BEC cross-over in a cold dilute gas of ^{40}K. The most general many-body Hamiltonian, including all atomic internal degrees of freedom, has the following form:

$$\hat{H}_{\mathrm{MB}} = \sum_{\nu_1,\mathbf{k}} \epsilon_{\mathbf{k},\nu_1} \hat{a}^{\dagger}_{\mathbf{k},\nu_1} \hat{a}_{\mathbf{k},\nu_1} + \frac{1}{2} \sum_{\nu_1,\nu_2,\nu_3,\nu_4} \sum_{\mathbf{k},\mathbf{k}',\mathbf{q}} V_{\nu_1,\nu_2,\nu_3,\nu_4}(\mathbf{k},\mathbf{k}') \times \hat{a}^{\dagger}_{\frac{\mathbf{q}}{2}+\mathbf{k},\nu_1} \hat{a}^{\dagger}_{\frac{\mathbf{q}}{2}-\mathbf{k},\nu_2} \hat{a}_{\frac{\mathbf{q}}{2}-\mathbf{k}',\nu_3} \hat{a}_{\frac{\mathbf{q}}{2}+\mathbf{k}',\nu_4} \,. \tag{25}$$

Here the indices ν_1, ν_2, ν_3, ν_4 label the atomic Zeeman levels. The wave vector $\mathbf{k}$ in the kinetic energy contribution to Eq. (25) is associated with a single-particle momentum, while the pairs of wave vectors $\mathbf{q}$ and $\mathbf{k}$ in the interaction term correspond to two-body centre-of-mass and relative momenta. All these indices refer to our choice of plane wave basis states $\exp(i\mathbf{k}\cdot\mathbf{r})/\sqrt{\mathcal{V}}$ in a box of volume $\mathcal{V}$ with periodic boundary conditions. The associated annihilation and creation operators obey the usual fermionic anti-commutation relations:

$$\hat{a}_{\mathbf{k},\nu_1}\hat{a}^{\dagger}_{\mathbf{k}',\nu_2} + \hat{a}^{\dagger}_{\mathbf{k}',\nu_2}\hat{a}_{\mathbf{k},\nu_1} = \delta_{\nu_1,\nu_2}\delta_{\mathbf{k},\mathbf{k}'} \,, \tag{26}$$

$$\hat{a}_{\mathbf{k},\nu_1}\hat{a}_{\mathbf{k}',\nu_2} + \hat{a}_{\mathbf{k}',\nu_2}\hat{a}_{\mathbf{k},\nu_1} = 0 \,. \tag{27}$$

We note that the microscopic potentials $V_{\nu_1,\nu_2,\nu_3,\nu_4}$ in Eq. (25) all decay to zero in the limit of large inter-atomic separation. The atomic Zeeman energies, which determine the dissociation thresholds of the different two-body asymptotic scattering channels are included in the single-particle energies $\epsilon_{\mathbf{k},\nu_1}$.

B. Ambiguities between different many-body approaches

While a mean-field treatment of the BCS-BEC cross-over using realistic microscopic interactions for all binary scattering channels seems impractical, there are several ways to formulate approximate theories, derived from the Hamiltonian of Eq. (25) or the effective boson-fermion model [17, 18], which are all compatible with the two-channel approach to the binary collision physics of Section II. One possible condition for such a compatibility may be, for instance, that the binding energy of the Feshbach molecule, predicted by the two-channel approach, exactly coincides with twice the chemical potential obtained from the mean-field theory in the asymptotic limit of zero density.

During the course of our studies we have derived such a mean-field approach [39], based on the microscopic Hamiltonian of Eq. (25) and the general kinetic theory of Refs. [40, 41], by applying the two-channel approach of Section II, including the single-resonance approximation, to the two-body propagators. This treatment is most sensible as it relies upon controlled approximations rather than uncontrollable model assumptions about the form of an effective Hamiltonian. The dynamic equations for the one-body density matrix, however, explicitly depend on the single-atom Zeeman states that constitute the closed channel associated with the Feshbach resonance level. The atomic energy levels need to be explicitly specified in such a description once one and the same single-particle Zeeman state is shared between the relevant two-body entrance and closed channels. This phenomenon has been discussed previously in Ref. [42] for the case of ^{40}K and reflects physical intuition, since measurements of single-particle quantities, like the position of an atom or its internal state, do not necessarily provide information about whether this atom was correlated with another partner in the spatial configuration of the Feshbach resonance level.

The assumption of such a generally unphysical possibility of distinguishing spatially separated from correlated atom pairs in a gas on the basis of one-body observables underlies the boson-fermion model [17, 18]. This model separates out the Feshbach resonance state on the level of the Hamiltonian. We shall show, however, that the standard thermodynamic physical quantities we discuss in Section V are recovered, at least on the level of the mean-field approximation, by many-body approaches based on both the boson-fermion and the standard fermionic Hamiltonians, provided that they are suitably adjusted to be compatible with the precise two-channel approach to the two-body physics of Section II. This observation suggests that the thermal equilibrium properties of Section V are insensitive to the underlying model Hamiltonian, regardless of the level of accuracy to which they include the separation into different asymptotic binary scattering channels.

C. Adjustment of the boson-fermion model

The boson-fermion model leads to an effective two-channel description of the two-body physics and includes only the interactions between unlike fermions in the different Zeeman states associated with the entrance channel of Section II. The boson-fermion Hamiltonian has the following form:

$$\begin{aligned}\hat{H}_{\mathrm{MB-BF}} = &\sum_{s,\mathbf{k}} \epsilon_{\mathbf{k}} \hat{a}^{\dagger}_{\mathbf{k},s} \hat{a}_{\mathbf{k},s} + \sum_{\mathbf{q}} \left[E_{\mathbf{q}} + E_{\mathrm{res}}(B)\right] \hat{b}^{\dagger}_{\mathbf{q}} \hat{b}_{\mathbf{q}} \\ &+ \sum_{\mathbf{k},\mathbf{k}',\mathbf{q}} V_{\mathrm{bg}}(\mathbf{k},\mathbf{k}') \hat{a}^{\dagger}_{\frac{\mathbf{q}}{2}+\mathbf{k},\uparrow} \hat{a}^{\dagger}_{\frac{\mathbf{q}}{2}-\mathbf{k},\downarrow} \hat{a}_{\frac{\mathbf{q}}{2}-\mathbf{k}',\downarrow} \hat{a}_{\frac{\mathbf{q}}{2}+\mathbf{k}',\uparrow} \\ &+ \sum_{\mathbf{k},\mathbf{q}} g(\mathbf{k}) \left(\hat{b}^{\dagger}_{\mathbf{q}} \hat{a}_{\frac{\mathbf{q}}{2}-\mathbf{k},\downarrow} \hat{a}_{\frac{\mathbf{q}}{2}+\mathbf{k},\uparrow} + h.c. \right) . \end{aligned} \tag{28}$$

Here $\hat{b}_{\mathbf{q}}$ and $\hat{b}^{\dagger}_{\mathbf{q}}$ annihilate or create pairs of atoms with the centre-of-mass momentum $\mathbf{q}$ in the Feshbach resonance level, respectively, and fulfil the bosonic commutation relations:

$$\hat{b}_{\mathbf{q}} \hat{b}^{\dagger}_{\mathbf{q}'} - \hat{b}^{\dagger}_{\mathbf{q}'} \hat{b}_{\mathbf{q}} = \delta_{\mathbf{q},\mathbf{q}'} , \tag{29}$$

$$\hat{b}_{\mathbf{q}} \hat{b}_{\mathbf{q}'} - \hat{b}_{\mathbf{q}'} \hat{b}_{\mathbf{q}} = 0 . \tag{30}$$

The kinetic energy associated with the centre of mass of an atom pair in the meta-stable Feshbach resonance level is denoted by $E_{\mathbf{q}}$. In analogy to related applications in the theory of superconductivity, we choose, in the following, the notation $s =\uparrow,\downarrow$ to label the single-particle Zeeman levels that constitute the s-wave entrance channel. We assume all fermionic operators $\hat{a}_{\mathbf{k},s}$ and $\hat{a}^{\dagger}_{\mathbf{k},s}$ to commute with all bosonic operators $\hat{b}_{\mathbf{q}}$ and $\hat{b}^{\dagger}_{\mathbf{q}}$. In analogy to our considerations of the two-body problem in Section II we have included the magnetic field dependent single-particle Zeeman energies in the binary interactions. The single-particle energies $\epsilon_{\mathbf{k}}$ are therefore independent of the index s associated with atomic Zeeman levels.

In order to determine the parameters of the boson-fermion Hamiltonian, we compare the Schrödinger equations obtained from Eq. (28) and the binary two-channel Hamiltonian of Eq. (2) when applied to a general two-body state with components in both the entrance channel and the Feshbach resonance level. As both approaches are required to describe the same physics, this comparison shows that $E_{\mathrm{res}}(B)$ is the resonance energy given by Eq. (8), while V_{bg} is the background scattering potential of Eq. (3). Its matrix element in terms of the energy states of the periodic box is thus given by

$$V_{\mathrm{bg}}(\mathbf{k},\mathbf{k}') = \frac{1}{\mathcal{V}} \int_{\mathcal{V}} d\mathbf{r} \int_{\mathcal{V}} d\mathbf{r}'\, e^{-i\mathbf{k}\cdot\mathbf{r}} V_{\mathrm{bg}}(\mathbf{r},\mathbf{r}') e^{i\mathbf{k}'\cdot\mathbf{r}'} , \tag{31}$$

where the integration extends over the volume $\mathcal{V}$ of the box. The parameter

$$g(\mathbf{k}) = \frac{1}{\sqrt{\mathcal{V}}} \int_{\mathcal{V}} d\mathbf{r}\, e^{-i\mathbf{k}\cdot\mathbf{r}} W(r) \phi_{\mathrm{res}}(r) , \tag{32}$$

which characterises the inter-channel coupling, can be obtained from Eq. (9). We note that with these adjustments of potentials and parameters the boson-fermion Hamiltonian of Eq. (28) and the two-channel approach in the single resonance approximation of Section II provide exactly identical descriptions of the two-body physics.

D. Adjustment of the standard fermionic Hamiltonian

A many-body approach compatible with the single-channel description of resonance enhancement in the binary low energy collision physics of Section II can be obtained from a many-body Hamiltonian usually applied in the theory of superconductivity [3, 4, 23]. This standard fermionic Hamiltonian is given by the following expression:

$$\begin{aligned}\hat{H}_{\mathrm{MB-F}} = &\sum_{s,\mathbf{k}} \epsilon_{\mathbf{k}} \hat{a}^{\dagger}_{\mathbf{k},s} \hat{a}_{\mathbf{k},s} + \sum_{\mathbf{k},\mathbf{k}',\mathbf{q}} V_{\mathrm{eff-1ch}}(\mathbf{k},\mathbf{k}',B) \\ &\times \hat{a}^{\dagger}_{\frac{\mathbf{q}}{2}+\mathbf{k},\uparrow} \hat{a}^{\dagger}_{\frac{\mathbf{q}}{2}-\mathbf{k},\downarrow} \hat{a}_{\frac{\mathbf{q}}{2}-\mathbf{k}',\downarrow} \hat{a}_{\frac{\mathbf{q}}{2}+\mathbf{k}',\uparrow} . \end{aligned} \tag{33}$$

Here $V_{\mathrm{eff-1ch}}(B)$ is the interaction potential for a pair of atoms in the Zeeman states associated with the entrance channel, which we have labelled by the indices $s =\uparrow,\downarrow$. We choose this potential to be identical to the binary interaction in the single-channel Hamiltonian of Eq. (22). This choice assures that the two-body physics described by the standard fermionic Hamiltonian exactly agrees with the single-channel approach of Section II.

As both the two- and single-channel approaches of Section II yield virtually the same low energy two-body physics, we may also expect a similar agreement between the predictions obtained from the Hamiltonians of Eqs. (28) and (33) with regard to the thermal equilibrium physical quantities of Section V. The formal establishment of this equivalence of these many-body Hamiltonians in applications to standard mean-field theory will be the subject of the following sections. Since we have included smooth binary potentials with a proper spatial extent in the Hamiltonians, our mean-field calculations do not involve ultra-violet divergences and, therefore, do not require any renormalisation procedures.

IV. MEAN-FIELD APPROACH TO THE THERMAL EQUILIBRIUM

At temperatures close to absolute zero or well below the critical temperature T_c, the BCS-BEC cross-over has been successfully analysed by mean-field theory in terms of the BCS wave function, which smoothly interpolates between the BCS and BEC regimes [1, 3, 5]. The derivation of the thermal equilibrium properties [32, 33, 43, 44, 45, 46, 47, 48, 49, 50, 51, 52, 53, 54, 55, 56, 57, 58, 59, 60, 61, 62, 63, 64, 65] follows standard techniques (see, e.g., Ref. [23]). We thus include just a brief derivation of their extension to the boson-fermion model, applying path integral methods [66]. The associated mean-field approach for the standard fermionic Hamiltonian model can be obtained from our analysis simply by replacing $g(\mathbf{k}) \to 0$ and $V_{\rm bg} \to V_{\rm eff-1ch}$ in all formulae.

A. Path integral approach

All thermodynamic equilibrium physical quantities of a gas can be derived from the quantum partition function, which is given by the general formula:

$$\mathcal{Z} = \mathrm{tr}\left[e^{-\beta\left(\hat{H}_{\rm MB-BF}-\mu\hat{N}\right)}\right]. \tag{34}$$

Here the factor $\beta = 1/(k_{\rm B}T)$ accounts for the temperature T scaled to energy units by the Boltzmann constant $k_{\rm B}$, $\hat{N}$ is the number operator and μ the chemical potential, while “tr” indicates the trace of an operator. The quantum partition function $\mathcal{Z}$ can be conveniently represented in terms of a coherent state path integral. To this end, we introduce the action

$$S = \int_0^\beta d\tau \left(H_{\rm MB-BF} - \sum_{\mathbf{q}} \bar{b}_{\mathbf{q}}\partial_\tau b_{\mathbf{q}} - \sum_{\mathbf{k}} \bar{\psi}_{\mathbf{k}}\partial_\tau\psi_{\mathbf{k}} - \mu N \right), \tag{35}$$

where N is the total number of atoms and $H_{\rm MB-BF}$ is the many-body boson-fermion Hamiltonian of Eq. (28). In this Hamiltonian $\hat{a}_{\mathbf{k},s}$ and $\hat{b}_{\mathbf{q}}$ are replaced by τ-dependent Grassmann numbers $a_{\mathbf{k},s}$ and c-numbers $b_{\mathbf{q}}$, respectively. We have, furthermore, introduced the quantities $\bar{a}_{\mathbf{k},s}$, $\bar{b}_{\mathbf{q}}$ as well as the Nambu spinors

$$\psi_{\mathbf{k}} = \begin{pmatrix} a_{\mathbf{k},\uparrow} \\ \bar{a}_{-\mathbf{k},\downarrow} \end{pmatrix}, \; \bar{\psi}_{\mathbf{k}} = (\bar{a}_{\mathbf{k},\uparrow}, a_{-\mathbf{k},\downarrow}) \tag{36}$$

in Eq. (35), where the bar indicates that the quantities $\bar{a}_{\mathbf{k},s}$ and $a_{\mathbf{k},s}$, etc., are independently varied. In our considerations $\bar{a}_{\mathbf{k},s}$ and $a_{\mathbf{k},s}$ as well as $b_{\mathbf{q}}$ and $\bar{b}_{\mathbf{q}}$ are all related by complex conjugation. The coherent state path integral then determines quantum partition function $\mathcal{Z}$ in terms of the action to be:

$$\mathcal{Z} = \int D(\bar{\psi}, \psi, \bar{b}, b) e^{-S} \,. \tag{37}$$

B. Relationship between the path integral approach and the zero-temperature mean-field approximation

In the following, we shall briefly summarise the assumptions underlying our evaluation of Eq. (37) in the mean-field approximation as well as their relationship to derivations based on the condensate wave function of Refs. [1, 3, 5]. In order to treat the interaction we isolate the components associated with the pairing. Such a procedure is equivalent to considering only those contributions of the total Hamiltonian that yield non-zero matrix elements in the condensate state, i.e., $\langle\Phi|\hat{H}_{\rm MB-BF}|\Phi\rangle \neq 0$. Following the ideas of standard BCS theory [23], the associated zero-temperature ground state condensate wave function is given by the formula:

$$\begin{aligned} |\Phi\rangle &= \frac{\exp\left(-|\lambda_{\rm b}|^2/2 + \lambda_{\rm b}\hat{b}_0^\dagger + \sum_{\mathbf{k}} w_{\mathbf{k}}\hat{a}^\dagger_{\mathbf{k},\uparrow}\hat{a}^\dagger_{-\mathbf{k},\downarrow}\right)}{\prod_{\mathbf{k}'}\left(1+|w_{\mathbf{k}'}|^2\right)^{1/2}}|\mathrm{vac}\rangle \\ &= e^{-|\lambda_{\rm b}|^2/2+\lambda_{\rm b}\hat{b}_0^\dagger}\prod_{\mathbf{k}}\left(u_{\mathbf{k}} + v_{\mathbf{k}}\hat{a}^\dagger_{\mathbf{k},\uparrow}\hat{a}^\dagger_{-\mathbf{k},\downarrow}\right)|\mathrm{vac}\rangle \,. \end{aligned} \tag{38}$$

Here $|\mathrm{vac}\rangle$ is the vacuum state. We have, furthermore, introduced the quantity $w_{\mathbf{k}} = v_{\mathbf{k}}/u_{\mathbf{k}}$ in Eq. (38) which depends on the quasi-particle amplitudes $u_{\mathbf{k}}$ and $v_{\mathbf{k}}$. The quasi-particle amplitudes fulfil the requirement $|u_{\mathbf{k}}|^2 + |v_{\mathbf{k}}|^2 = 1$, where

$$2\,|v_{\mathbf{k}}|^2 = \langle\Phi|\left(\hat{a}^\dagger_{\mathbf{k},\uparrow}\hat{a}_{\mathbf{k},\uparrow} + \hat{a}^\dagger_{\mathbf{k},\downarrow}\hat{a}_{\mathbf{k},\downarrow}\right)|\Phi\rangle \tag{39}$$

determines the average occupation number of the momentum mode associated with the wave vector $\mathbf{k}$. The product $\kappa_{\mathbf{k}} = u_{\mathbf{k}}v_{\mathbf{k}}$ can be interpreted as a pair wave function, whose modulus squared, summed over all wave vectors $\mathbf{k}$ (i.e. $\sum_{\mathbf{k}}|u_{\mathbf{k}}v_{\mathbf{k}}|^2$), provides a measure for the number of condensed fermionic pairs. Within the framework of the boson-fermion model, the coefficient $\lambda_{\rm b}$ in Eq. (38) is related to the average number of pairs of atoms in the resonance state configuration through the formula:

$$|\lambda_{\rm b}|^2 = \langle\Phi|\hat{b}_0^\dagger\hat{b}_0|\Phi\rangle \,. \tag{40}$$

We shall omit, in our evaluation of Eq. (37), the decoupling in the diagonal, Hartree-Fock, channel because, firstly, the Fock pairing, which results from exchange, requires indistinguishable atoms in the same Zeeman states. The associated binary interactions, however, which all involve non-isotropic partial waves, are omitted from the outset in the s-wave boson-fermion Hamiltonian. Secondly, the inclusion of the Hartree term results in only a negligible energy shift.

C. Hubbard-Stratonovich transformation

To further evaluate the finite temperature partition function of Eq. (37), we proceed by applying the Hubbard-Stratonovich decoupling to the interaction in the off-diagonal channel, which yields:

$$\mathcal{Z} = \int D(\bar{\psi}, \psi, \bar{b}_0, b_0) \int D(\Delta^*, \Delta) \exp\left[\int_0^\beta d\tau \sum_{\mathbf{k}} \bar{\psi}_{\mathbf{k}} \begin{pmatrix} \partial_\tau - \epsilon_{\mathbf{k}} + \mu & -g(\mathbf{k}) b_0 - \Delta_{\mathbf{k}} \\ -g(\mathbf{k}) \bar{b}_0 - \Delta^*_{\mathbf{k}} & \partial_\tau + \epsilon_{\mathbf{k}} - \mu \end{pmatrix} \psi_{\mathbf{k}} - S_0 \right]. \tag{41}$$

The transformed partition function depends on the order parameter $\Delta_{\mathbf{k}}$, sometimes referred to as the Hubbard-Stratonovich field, whose explicit expression within the mean-field approximation in the limit of zero temperature reads $\Delta_{\mathbf{k}} = -\sum_{\mathbf{k}'} V_{\mathrm{bg}}(\mathbf{k}, \mathbf{k}') \langle \Phi | \hat{a}_{-\mathbf{k}',\downarrow} \hat{a}_{\mathbf{k}',\uparrow} | \Phi \rangle$. In our more general finite temperature treatment the order parameter is a τ-dependent function which we shall determine using a saddle-point analysis. We have, furthermore, introduced in Eq. (41) the quantity

$$\begin{aligned} S_0 = & \int_0^\beta d\tau \sum_{\mathbf{k},\mathbf{k}'} \Delta^*_{\mathbf{k}} V^{-1}_{\mathrm{bg}}(\mathbf{k}, \mathbf{k}') \Delta_{\mathbf{k}'} \\ & - \int_0^\beta d\tau\, \bar{b}_0 \left[\partial_\tau - E_{\mathrm{res}}(B) + 2\mu \right] b_0 \,, \end{aligned} \tag{42}$$

where V^{-1}_{bg} indicates the inverse potential energy operator associated with the background scattering in the relative motion of a pair of unlike fermions. We note that, in the mean-field approximation, the partition function of Eq. (41) depends only on the c-numbers $b_{\mathbf{q}=0}$ and $\bar{b}_{\mathbf{q}=0}$ associated with the zero-momentum mode of the centre-of-mass motion of a pair of fermions in the resonance level.

Since the exponent in Eq. (41) is a quadratic form in the fermionic fields, the associated Gaussian integral can be performed straightforwardly. This integration leads to the following formula:

$$\mathcal{Z} = \int D(\Delta^*, \Delta, \bar{b}_0, b_0) e^{-S_0} \exp\left(\mathrm{tr}\left[\ln G^{-1} \right] \right) . \tag{43}$$

This formula depends on the thermal Green's function G, whose inverse operator is given by:

$$\begin{aligned} G^{-1} = & \partial_\tau - (\epsilon_{\mathbf{k}} - \mu)\, \sigma_3 - \left[g(\mathbf{k}) b_0 + \Delta_{\mathbf{k}} \right] \sigma_+ \\ & - \left[g(\mathbf{k}) \bar{b}_0 + \Delta^*_{\mathbf{k}} \right] \sigma_- \,. \end{aligned} \tag{44}$$

Here σ_1, σ_2 and σ_3 are the usual two-dimensional Pauli spin matrices, i.e. their commutation relations are given by $\sigma_1\sigma_2 - \sigma_2\sigma_1 = 2i\sigma_3$ and its cyclic permutations, while $\sigma_+ = (\sigma_1 + i\sigma_2)/2$ and $\sigma_- = (\sigma_1 - i\sigma_2)/2$ are the associated raising and lowering matrices.

D. Saddle-point analysis

We shall apply, in the following, a saddle-point analysis in which the order parameters $\Delta_{\mathbf{k}}(\tau)$ and $b_0(\tau)$ are assumed to be independent of τ. This approach minimises the free energy as the derivatives of $\Delta_{\mathbf{k}}$ and b_0, with respect to τ, do not contribute. The Green's function G is then diagonal in the Matsubara frequencies and in the wave vectors $\mathbf{k}$. We shall, therefore, employ a discrete Fourier analysis to change the representation from the variable τ to the Matsubara frequencies $\omega_j = (2j+1)\pi/\beta$, where j is an integer. Performing the Fourier expansion of G^{-1}, after inversion, the mean-field thermal Green's function is given by the formula:

$$\begin{aligned} G_{\mathbf{k}\omega_j} = & \frac{1}{\omega_j^2 + E_{\mathbf{k}}^2} \Big\{ - i\omega_j - (\epsilon_{\mathbf{k}} - \mu)\sigma_3 - \left[g(\mathbf{k}) b_0 + \Delta_{\mathbf{k}} \right] \sigma_+ \\ & - \left[g(\mathbf{k}) \bar{b}_0 + \Delta^*_{\mathbf{k}} \right] \sigma_- \Big\} . \end{aligned} \tag{45}$$

Here $E_{\mathbf{k}} = \sqrt{(\epsilon_{\mathbf{k}} - \mu)^2 + |g(\mathbf{k}) b_0 + \Delta_{\mathbf{k}}|^2}$ are the single-particle excitation energies. Varying the action with respect to $\Delta^*_{\mathbf{k}}$ and $\bar{b}_0$ leads to the saddle-point (mean-field) equations. We then perform the standard Matsubara frequencies summation and consider the uniform gas limit, obtained by the following substitution $\sum_{\mathbf{k}} \to \int \mathcal{V} \frac{d\mathbf{k}}{(2\pi)^3} = \int \mathcal{V} \frac{d\mathbf{p}}{(2\pi\hbar)^3}$. In the following, we shall use the explicit form of the potentials of Section II, i.e. the background scattering potential $V_{\mathrm{bg}}(p, p') = \xi_{\mathrm{bg}} \chi_{\mathrm{bg}}(p) \chi_{\mathrm{bg}}(p')$ and the inter-channel coupling $g(p) = \zeta \chi(p)$, in addition to the abbreviation

$$\int d\mathbf{p}\, \chi_{\mathrm{bg}}(p) \Delta_p = \xi_{\mathrm{bg}} \Delta \,. \tag{46}$$

The saddle-point equations are then given by the following pair of formulae:

$$\Delta = \int d\mathbf{p} \frac{\chi_{\mathrm{bg}}(p) \Sigma(p)}{2\sqrt{(\epsilon_p - \mu)^2 + |\Sigma(p)|^2}} \tanh\left(\frac{\beta E_p}{2} \right), \tag{47}$$

$$\left[E_{\mathrm{res}}(B) - 2\mu \right] b_0 = \int d\mathbf{p} \frac{\zeta \chi(p) \Sigma(p)}{2\sqrt{(\epsilon_p - \mu)^2 + |\Sigma(p)|^2}} \tanh\left(\frac{\beta E_p}{2} \right). \tag{48}$$

Here the quantity

$$\Sigma(p) = \zeta \chi(p) b_0 + \xi_{\mathrm{bg}} \chi_{\mathrm{bg}}(p) \Delta \tag{49}$$

may be interpreted as a self energy. The chemical potential μ is determined by the density equation

$$n = \frac{1}{(2\pi\hbar)^3} \left[2\bar{b}_0 b_0 + \int d\mathbf{p} \left(1 - \frac{\epsilon_p - \mu}{\sqrt{(\epsilon_p - \mu)^2 + |\Sigma(p)|^2}} \right) \right], \tag{50}$$

where n is the number of atoms per unit volume. The mean-field partition function reads:

$$\mathcal{Z}_{\mathrm{MF}} = e^{-S_0} \exp\left(\mathrm{tr}\left[\ln G^{-1} \right] \right) . \tag{51}$$

Here S_0 and G^{-1}, given by Eqs. (42) and (44), respectively, are now evaluated at the saddle point, i.e. b_0 and Δ are the solutions of Eqs. (47), (48) and (50).

E. Solutions of the saddle-point equations

In Section V we provide the numerical solutions of the three coupled equations (47), (48) and (50). To obtain a qualitative overview of their behaviour, we note that in the zero-density limit $n \to 0$ the chemical potential μ recovers half the molecular binding energy and the equations (47), (48) and (50) reduce to the two-body Schrödinger equation associated with the two-channel Hamiltonian (2). There are, however, two different solutions to this equation. One of them corresponds to the weakly bound Feshbach molecular state just below the entrance channel dissociation threshold (solid curve in Figure 1). This state can be efficiently populated by an adiabatic sweep of the magnetic field strength. The second solution corresponds to the next, more tightly bound, molecular state of energy given by the dashed curve in Figure 1. Similarly, at the many-body level (i.e. $n \neq 0$) there are three different extrema of the effective action in Eq. (43), which are all solutions of Eqs. (47), (48) and (50) associated with different chemical potentials. The trivial uncondensed solution ($\Delta = 0$, $b_0 = 0$) is unstable below T_c, but there are two stable solutions with a finite condensate component. One of them corresponds to the condensation of weakly bound Feshbach molecules with an energy just below the entrance channel dissociation threshold (solid curve in Figure 1). The other solution corresponds to the condensation of molecules in the more tightly bound state (dashed curve in Figure 1). The latter solution is given by a lower minimum of the effective action in Eq. (43), but it is not populated on the time scale of the experiments of Ref. [9]. Instead, the local minimum (quasi-equilibrium) solution is the physical one, relevant to the experiments of Ref. [9]. We shall analyse this solution in Section V.

The saddle-point equations for the mean-field approach associated with the standard fermionic Hamiltonian of Eq. (33) can be easily obtained from Eqs. (47), (48) and (50) in the limit $g(p) \to 0$, in addition to the replacement $V_\mathrm{bg} \to V_{\mathrm{eff-1ch}}$. The single-channel effective potential $V_{\mathrm{eff-1ch}}$ supports just a single bound state, the Feshbach molecule, which is efficiently populated in the experiments of Ref. [9]. The associated mean-field equations, therefore, have only two solutions: the uncondensed one, unstable below T_c, and the condensate of weakly bound molecules, which we shall analyse in Section V.

V. BCS-BEC CROSS-OVER IN A DILUTE ^{40}K GAS

Using the microscopic parameters determined in Section II, we have numerically solved the coupled saddle-point equations (47), (48) and (50) for a wide range of magnetic fields and atomic densities. In particular, we have considered magnetic field strengths from 1 G above to 10 G below the position of the zero-energy resonance ($B_0 = 202.1$ G [9]) in a mixture of fermionic ^{40}K atoms in ($f = 9/2, m_f = -9/2$) and ($f = 9/2, m_f = -7/2$) Zeeman states. This range covers all magnetic field strengths relevant to Ref. [9] and includes both the universal regime around the zero-energy resonance (extending to about 1 G below B_0) and the region in which the energy of the Feshbach molecule is strongly influenced by the anti-crossing between the energies of the two highest excited diatomic multi-channel vibrational bound states (solid and dashed curves in Fig. 1). We have also considered a wide range of experimentally accessible densities from 10^{12} cm^{-3} to 5×10^{14} cm^{-3}. In order to establish a characteristic value of the density of atoms in a homogeneous two-component gas, we require it to reproduce the Fermi energy of the trapped gas for the conditions of Ref. [9]. This characteristic density is equal to 1.5×10^{13} cm^{-3} and is given by the two-component peak density of atoms in the trap.

A. Standard fermionic versus boson-fermion approach

We have performed the numerical analysis for both approaches, using the standard fermionic Hamiltonian and the boson-fermion Hamiltonian, and found that in the entire range of experimentally relevant magnetic field strengths and densities there is hardly any difference visible between them for the standard many-body observables considered in this paper. Consequently, in the following discussion, we just give the results obtained from the standard fermionic Hamiltonian and explicitly point out small differences with respect to the boson-fermion approach when they arise.

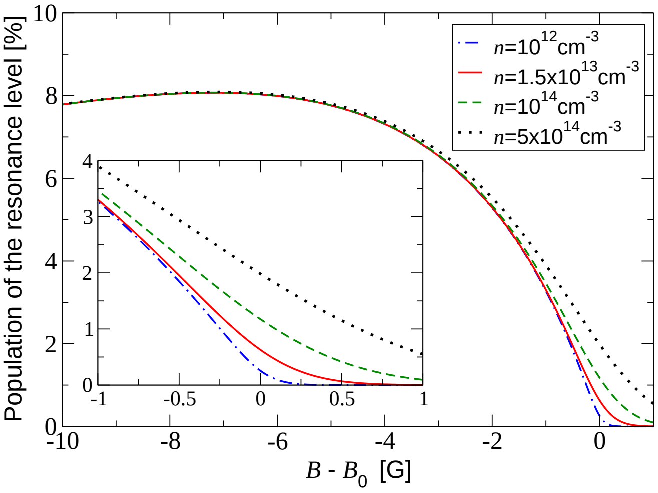

FIG. 3: (Color online) The fraction of the population associated with the Feshbach resonance level of the closed channel as a function of the magnetic field strength B and the density n. The solid curve corresponds to the density characteristic for the experiment of Ref. [9] while the result for the lowest density studied (the dot-dashed curve) is practically indistinguishable from the closed-channel admixture to the coupled-channels bound state wave function of the two-body problem. The inset enlarges the region in the vicinity of the zero-energy resonance. We note that, regardless of the density, the maximum population associated with the bosonic field operator b_0 is only 8% for $B - B_0 \approx -7.2$ G. Given the virtual density independence of this maximum population, this result also coincides with the maximum closed-channel admixture to the highest-excited vibrational diatomic bound state of the two-channel two-body Hamiltonian (2).

At the two-body level, the similarity of the results obtained from both many-body approaches is principally due to the fact that the admixture of the closed channel configuration to the highest excited multi-channel vibrational bound state is rather small for the entire range of experimentally relevant magnetic field strengths. In the many-body analysis of the boson-fermion approach this phenomenon is reflected in the small population associated with the bosonic field operator b_0, as shown in Figure 3. In the vicinity of the position of the zero-energy resonance (i.e. for magnetic field strength differences $B - B_0$ from -1 G to 1 G) this population exhibits some density dependence, but its magnitude is always less than 4%. In particular, for the density relevant to the experiment of Ref. [9] the Feshbach resonance population above B_0 reaches at most 0.6%, which is about one order of magnitude lower than the predictions of Refs. [32, 33]. Further below B_0, it becomes essentially density independent and reaches a maximum of about 8% at 7.2 G below the zero-energy resonance. This result agrees with the predictions of two-body coupled-channels calculations [28]. For even smaller values of the magnetic field strength the population associated with b_0 decreases. At the two-body level, this phenomenon stems from the influence of the anti-crossing between the two highest excited vibrational bound states (solid and dashed curves in Figure 1). The domination of the entrance channel components in the states of weakly-bound molecules reflects their long-range nature [22].

B. Pair wave function and single-particle excitation spectra

Several theoretical studies [1, 2, 3] have predicted that the cross-over between the BCS phase of correlated fermion pairs and the BEC phase of tightly bound diatomic molecules may be realised either by increasing the strength of the inter-particle interactions (the route employed in dilute Fermi gases) or by decreasing the particle density (as in the case of exciton and polariton BECs). In the following, we shall illustrate, as a function of density and interaction strength, the different pairing phenomena in terms of thermal equilibrium physical quantities that can be derived from the mean field approach of Section IV. We shall show, in particular, that the BCS-BEC cross-over point (zero of the chemical potential) in the experiments of Ref. [9] is shifted with respect to the position of the zero-energy resonance (singularity of the two-body scattering length) towards lower magnetic field strengths. This observation corroborates the conventional character of the BCS-BEC cross-over in ^{40}K as opposed to the ideas of resonance superfluidity outlined in Refs. [32, 33].

The equilibrium quantities that we shall consider involve the pair wave function

$$\kappa_{\mathbf{k}} = u_{\mathbf{k}} v_{\mathbf{k}} = \frac{\Sigma(\mathbf{k})}{2\sqrt{(\epsilon_{\mathbf{k}} - \mu)^2 + |\Sigma(\mathbf{k})|^2}}, \qquad (52)$$

the fermionic distribution function

$$|v_{\mathbf{k}}|^2 = \frac{1}{2}\left[1 - \frac{\epsilon_{\mathbf{k}} - \mu}{\sqrt{(\epsilon_{\mathbf{k}} - \mu)^2 + |\Sigma(\mathbf{k})|^2}}\right], \qquad (53)$$

and the single-particle excitation spectrum

$$E_{\mathbf{k}} = \sqrt{(\epsilon_{\mathbf{k}} - \mu)^2 + |\Sigma(\mathbf{k})|^2}\,. \qquad (54)$$

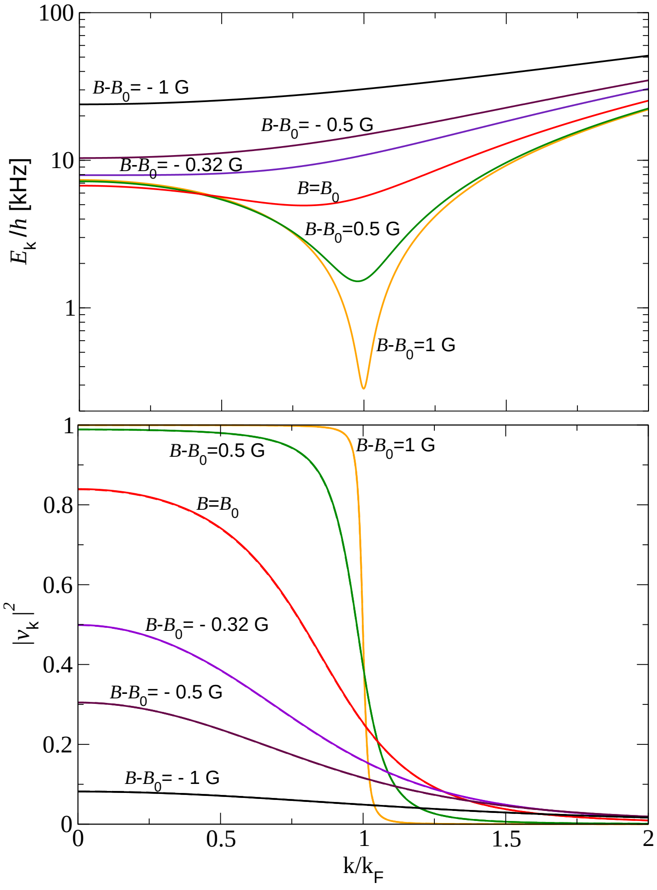

FIG. 4: (Color online) The single-particle excitation spectrum (the upper panel), given by Eq. (54), and the fermionic momentum distribution function (the lower panel), determined by Eq. (53), for the density $n = 1.5 \times 10^{13}$ cm^{-3} and a range of magnetic field strengths B, relevant to the experiment of Ref. [9]. We note that the minimum of the excitation spectrum evolves from its position at $k = k_{\mathrm{F}}$ on the BCS side to $k = 0$ at $B - B_0 = -0.32$ G.

The single-particle excitation spectra for densities of the experiment of Ref. [9] and different values of the magnetic field strength (the upper panel of Figure 4) show qualitatively different forms in the BEC and BCS limits of the cross-over problem. On the BCS side the excitation spectrum has a minimum at non-zero $k = k_{\mathrm{F}}$ (the two lower curves in the upper panel of Fig. 4), where k_{F} is the Fermi wave number. On the BEC side (the two upper curves in the upper panel of Fig. 4) $E_{\mathbf{k}}$ recovers the binding energy of a molecule at its minimum at $k = 0$. For finite wave numbers k the spectrum has a quadratic form associated with the dispersion relation of the kinetic energy of the molecules. We note that at a finite density the position of the zero-energy resonance B_0 is not a characteristic field strength with respect to the cross-over problem. In fact, at $B = B_0$ the spectrum shows BCS-like features due to its minimum at non-zero k. The value of the magnetic field strength where the minimum of the spectrum changes from non-zero to zero k depends on the density. In particular, for the density of the experiment of Ref. [9] this characteristic magnetic field strength is located at approximately 0.32 G below B_0. The fermionic momentum distribution function $|v_{\mathbf{k}}|^2$, as given by Eq. (53), is shown in the lower panel of Fig. 4. It smoothly evolves, as a function of the magnetic field strength, from the step-like form of a weakly-interacting Fermi gas (the BCS phase) towards a flat distribution characteristic for the macroscopic occupation of the lowest energy mode in a condensed Bose gas (the BEC phase). The qualitative change of pairing phenomena between the BCS and BEC limits is most intuitively reflected in the spatial form of the pair wave function. Its oscillatory behaviour on the BCS side is characteristic for unbound correlated pairs, while its exponential decay in the BEC limit recovers the long range asymptotic form of the molecular bound state wave function (see Fig. 5).

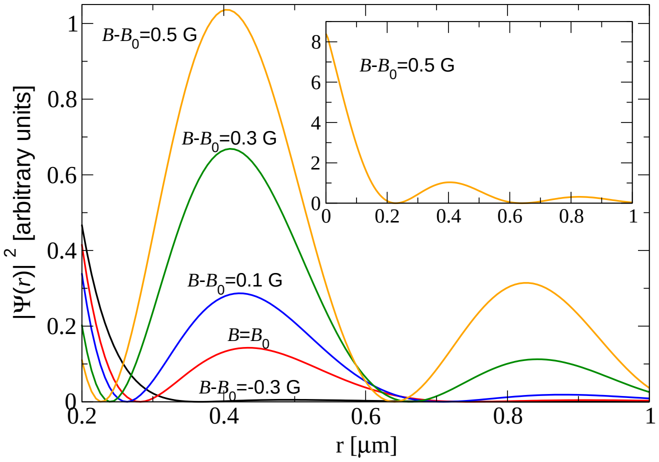

FIG. 5: (Color online) The spatial form of the pair wave function for the density $n = 1.5 \times 10^{13}$ cm^{-3} and a range of magnetic field strengths B. We note that for $B - B_0$ smaller than about -0.3 G the wave function loses its oscillatory form characteristic for the Cooper pairs and decays as a function of the inter-atomic distance. Such a virtually exponential decay is characteristic for diatomic bound states.

In the case of contact interactions, which are determined by a single parameter involving the scattering length, Leggett has shown [3] that the qualitative changes in the form of the pair wave function and the excitation spectrum occur when the chemical potential μ crosses zero. The chemical potential is positive on the BCS side and negative on the BEC side of the cross-over. In the case of spatially extended or non-local potentials (such as separable interactions) the qualitative change in the form of the pair wave function and the excitation spectra does not, in general, coincide with the vanishing of the chemical potential. Our results indicate, however, that in a dilute gas of ^{40}K atoms at typical experimentally accessible densities this boundary practically coincides with Leggett's universal boundary at $\mu = 0$. It is therefore instructive to study the chemical potential as a function of the magnetic field strength and as a function of the density (see Figure 6). Far below B_0 the chemical potential is negative, independent of the density and its limiting value recovers one half of the energy of the highest excited vibrational molecular bound state. The magnetic field strength where the chemical potential crosses zero (the cross-over point) depends on the density. Given the density $n = 1.5 \times 10^{13}$ cm^{-3}, characteristic for the experiments of Ref. [9], the cross-over point is located at 0.32 G below the position of the zero-energy resonance.

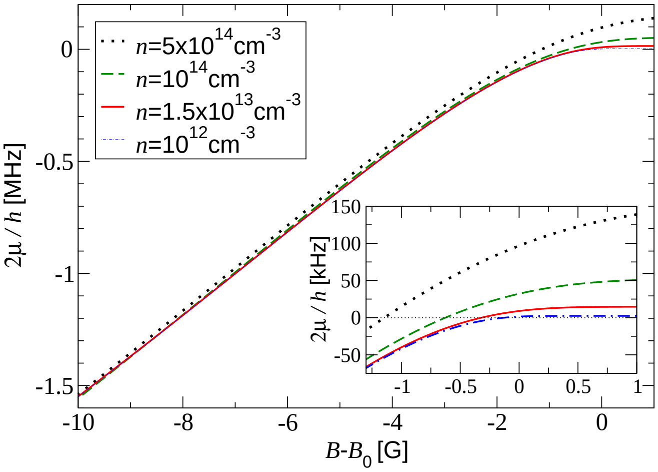

FIG. 6: (Color online) The chemical potential μ as a function of the magnetic field strength B for different densities n. Away from B_0, in the BEC limit, 2μ approaches the energy of the highest excited vibrational molecular bound state E_{b}, as depicted in Figure 2. We note that for the density $n = 1.5 \times 10^{13}$ cm^{-3} of the experiment [9] the chemical potential crosses zero at $B - B_0 = -0.32$ G. The inset enlarges the region in the vicinity of the zero-energy resonance.

To interpret the results of the pairwise projection technique employed in Ref. [9], we have also analysed the magnetic field and density dependences of the coherence length ξ. This typical length scale characterises the size of the fermionic pairs and is given by:

$$\xi^2 = \frac{\int d\mathbf{r}\, r^2\, [\kappa(r)]^2}{\int d\mathbf{r}\, [\kappa(r)]^2}\,. \tag{55}$$

Figure 7 shows the coherence length of the fermion pairs and the magnetic field strength for which the size of the pairs equals the mean inter-atomic spacing. For the characteristic density of the experiment of Ref. [9] the size of the fermion pairs equals the mean inter-atomic spacing at a magnetic field strength of about 0.5 G above the position of the zero-energy resonance. This coincides with the boundary value of the magnetic field strength at which condensation phenomena were observed via the pairwise projection technique employed in the experiments of Ref. [9].

C. Pairwise projection of fermionic condensates onto molecules

In the experiments of Ref. [9] a new method of probing the paired fermionic component of the gas was used. This

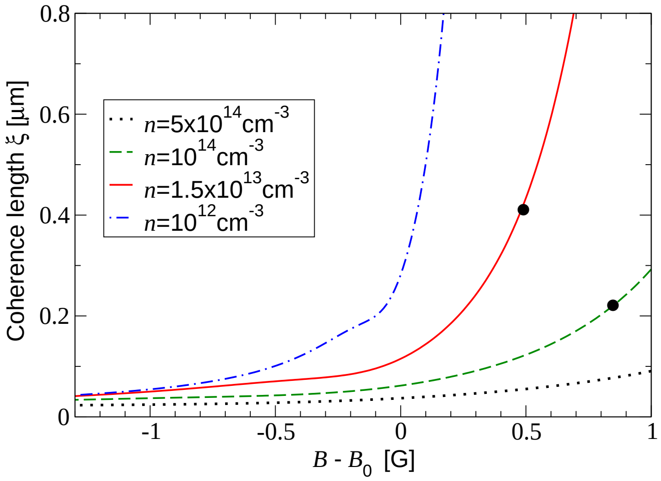

FIG. 7: (Color online) The coherence length ξ, characterising the size of the fermion pairs, as a function of the magnetic field strength B for different densities n. The circles indicate the values of the magnetic field strength at which the size of the pairs equals the mean inter-atomic spacing. We note that for the density $n = 1.5 \times 10^{13}$ cm^{-3} of the experiment of Ref. [9] (solid curve) the size of the pairs equals the mean inter-atomic spacing at $B \approx B_0 + 0.5$ G.

technique involved a fast ramp of the magnetic field strength across the 202 G resonance of ^{40}K. Ideally, this rapid process projects the centre-of-mass momentum distribution of the correlated fermionic pairs on the high field side of B_0 onto the centre-of-mass momentum distribution of weakly bound molecules on the low-field side of the zero-energy resonance [67]. Such a trapped fermionic condensate of correlated pairs is characterised by a narrow centre-of-mass momentum spread, which was indeed observed as a distinct peak in the measured molecular momentum distribution [9]. In the practical implementation of this procedure reported in Ref. [9], the magnetic field strength was swept to about 10 G below the position of the zero-energy resonance.

In order to gain further insight into the range of applicability of the experimental pairwise projection technique, we have analysed the critical temperature T_c for the BCS transition (depicted in Figure 8) as well as the fermionic condensate fraction f_c, i.e. the density of condensed pairs divided by one half of the total atomic density. This quantity f_c is thus given by

$$f_c = \frac{|b_0|^2 + \int d\mathbf{p}\, |\kappa_p|^2}{n/2} . \tag{56}$$

One of the measurable quantities in the pairwise projection technique is the density of condensed molecules observed after the fast sweep of the magnetic field strength below the position of the zero-energy resonance. For an idealised, i.e. instantaneous, sweep, this condensate density would be determined just by the projection of the initial pair wave function onto the wave function of the highest excited vibrational bound state $\phi_b(B_{\text{proj}})$ [i.e. an exact molecular bound state of the two-channel two-body Hamiltonian (2)] at the final magnetic field strength B_{proj}. This Feshbach molecular state becomes populated by the sweep. In the case of Ref. [9] the final magnetic field strength was $B_{\text{proj}} = B_0 - 10$ G. We have normalised the density of condensed molecules by a half of the atomic density n, in analogy to the definition of the fermionic condensate fraction of Eq. (56). This yields:

$$f_{\text{mol}} = \frac{\left| b_0/\mathcal{N}_b + \int d\mathbf{p}\, \kappa_p\, \phi_b^{\text{bg}}(p, B_{\text{proj}}) \right|^2}{n/2} , \tag{57}$$

where ϕ_b^{bg} is the entrance-channel component of the two-channel Feshbach molecular bound state given by Eq. (16) and $\mathcal{N}_b$ is the bound-state normalisation constant defined in Eq. (18). The fermionic condensate fraction f_c and its overlap f_{mol} with the bound state wave function $\phi_b(B_{\text{proj}})$ are shown in Fig. 9 (see also [60]).

As shown in Fig. 9, at the lowest experimentally reported [9] temperature of 0.08 T_F the fermionic condensate should be present up to about 0.6 G above the zero-energy resonance. For magnetic field strengths larger than about $B_0 + 0.5$ G, however, the overlap of the fermionic pair wave function with the target molecular wave function is negligible. Consequently, the paired fraction at higher magnetic fields is not detected by the pairwise projection technique, at least, under the idealising assumption that the magnetic field sweep is infinitely fast. The magnetic field strength at which the overlap of the paired fraction with the target molecular state vanishes also coincides with the field strength at which the extent of the pairs equals the mean inter-atomic spacing of the gas.

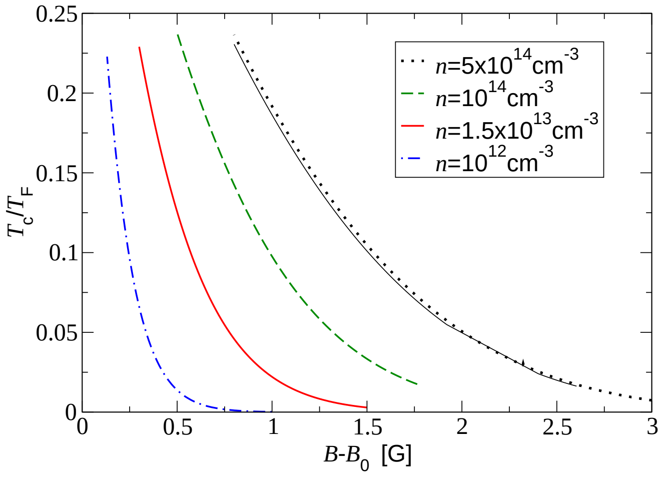

FIG. 8: (Color online) The critical temperature T_c for the BCS transition as a function of the magnetic field strength B for a range of densities n. The density of $n = 1.5 \times 10^{13}$ cm^{-3} corresponds to the Fermi temperature of $T_F = 0.35\,\mu$K quoted in Ref. [9]. We note the slight differences between the predictions of the boson-fermion (thin solid curve) and standard fermionic (dotted curve) for the highest density of $n = 5 \times 10^{14}$ cm^{-3}. This high-density critical temperature curve reflects the only calculation for which we were able to identify any visible differences between the two approaches.

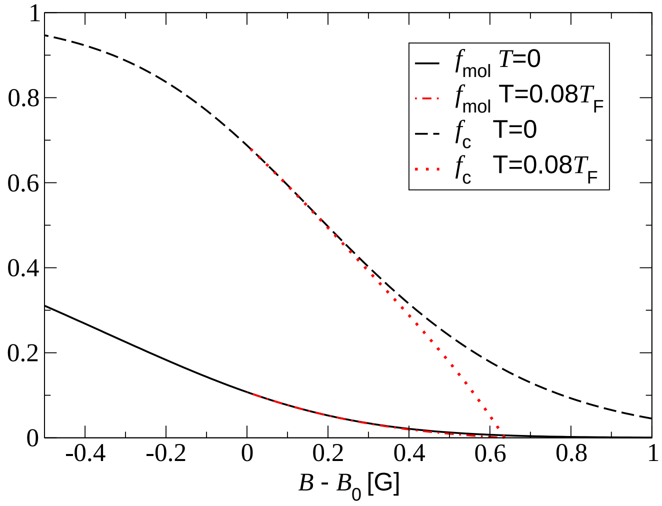

FIG. 9: (Color online) The fermionic condensate fraction $f_{\rm c}$ and its overlap $f_{\rm mol}$ with the target molecular bound state at 10 G below the zero-energy resonance for $T = 0$ (dashed and solid curves, respectively) and for $T = 0.08T_{\rm F}$ (dotted and dot-dashed curves, respectively). The density is $n = 1.5 \times 10^{13}$ cm^{-3} corresponding to the Fermi temperature of $T_{\rm F} = 0.35\mu$K quoted in Ref. [9].

VI. CONCLUSIONS

We have shown in this paper that the parameters of the general standard fermionic and boson-fermion many-body Hamiltonians, commonly used in studies of the BCS-BEC cross-over problem in dilute atomic gases, can be determined in an unambiguous manner by applying the Hamiltonians to a single pair of atoms and determining the low-energy binary bound state and scattering properties. In particular, we have described a convenient two-channel approach to the resonance enhanced two-body scattering, involving separable inter-atomic interactions. In a possible extension of this approach to the many-body description of a gas the five parameters of the boson-fermion Hamiltonian are all determined through five physical parameters of the resonance enhanced binary scattering, all of which can be deduced from measurements of binary scattering properties.

We have studied in detail the 202 G resonance in a mixture of $(f = 9/2, m_f = -9/2)$ and $(f = 9/2, m_f = -7/2)$ Zeeman states of ^{40}K fermions and shown that the maximum closed-channel admixture in the highest excited vibrational bound state reaches only about 8% at 7.2 G below the position of the zero-energy resonance. This small admixture is due to an avoided crossing between the energies of the Feshbach resonance level and a bound state of the background scattering potential. This points to the necessity of including the highest excited vibrational state of the background-scattering potential, in addition to the background scattering length, in the description of binary scattering in the vicinity of the zero-energy resonance relevant to the BCS-BEC cross-over. Including this second parameter characterising the entrance channel scattering also significantly extends the range of applicability of effective single channel approaches, a fact that often appears not to be appreciated. In fact, for the ^{40}K system studied in our paper we conclude that the energies of the highest-excited molecular bound state given by the effective single-channel approach are virtually indistinguishable from the results of a more elaborate two-channel analysis over the whole range of magnetic fields relevant to the experiment of Ref. [9]. The universal regime in the vicinity of the zero-energy resonance, however, where the binding energy is a function of the scattering length only, covers only a rather small fraction of the BCS-BEC regime in the case of ^{40}K.

These observations suggest that the effective single-channel approach with only two parameters should be sufficient also in studying the many-body BCS-BEC cross-over problem. To verify this, we have performed the mean-field analysis of the cross-over regime using the standard fermionic and the commonly used boson-fermion Hamiltonians for a wide range of atomic densities and magnetic fields. As anticipated, the results of our comparative studies remain virtually indistinguishable for all the many-body observables common to both types of Hamiltonians. The population associated with the bosonic field of the boson-fermion Hamiltonian remains, for the whole range of experimentally relevant densities, very close to the closed channel populations of the Feshbach molecule predicted by the two-body two-channel approach. In particular, in the regime where it reaches its maximum value of only about 8% (at 7.2 G below B_0) this quantity is already virtually density independent. For $B \geq B_0$ and the density of the experiment of Ref. [9] it remains below 0.6%, in stark contrast to the results of Refs. [32, 33]. We therefore conclude that for the ^{40}K system the standard fermionic many-body approach should be sufficient to study the whole BCS-BEC cross-over regime, as long as it properly accounts for the scattering length and the energy of the highest-excited vibrational bound state of the background-scattering potential.

Adjusting the parameters of the many-body Hamiltonian on the basis of the two-body considerations puts the proceeding analysis of the BCS-BEC cross-over problem of ^{40}K on firm ground. Adopting a different procedure may lead to unphysical conclusions. For example, one may reach a conclusion that below the zero-energy resonance there is a large population associated with the quantum field describing structureless bosons, as it appears in the boson-fermion Hamiltonian. One can also mistakenly associate this population with the number of the actually produced weakly-bound molecules. Such conclusions may result purely from ignoring the dominant influence of the background scattering potential and its highest excited vibrational bound state of energy E_{-1}. We have demonstrated that the background-scattering potential and its highest-excited vibrational bound state are crucial to a proper description of both two- and many-body physics outside the small universal regime in the vicinity of the zero-energy resonance.

We would also like to emphasise that the position B_0 of the zero-energy resonance, where the weakly bound molecular state emerges, is, due to strong inter-channel coupling, very different from the magnetic field strength $B_{\rm res}$ where the energy of the Feshbach resonance level $E_{\rm res}$ crosses the dissociation threshold of the entrance channel. In fact, for the ^{40}K resonance at $B_0 = 202.1$ G, $E_{\mathrm{res}}(B_0)$ is as large as $h\times 21.8$ MHz and negative. We note that the analyses of Refs. [32, 33] do not capture this important physical fact as they identify B_{res} with B_0.

Finally, we have analysed thermodynamic quantities associated with the BCS-BEC cross-over in ^{40}K. We found that for densities of the experiments of Ref. [9] the cross-over point, as characterised by a qualitative change in the form of the pair wave function from oscillatory to decaying and in the form of the single-particle excitation spectrum, takes place about 0.3 G below the position of the zero-energy resonance. We have also studied the pairwise projection technique employed in the experiment of Ref. [9] by calculating the overlap of the fermionic condensate wave function with the target molecular state at about 10 G below the zero-energy resonance. We found that when the fermionic pairs start to spatially overlap, which in the case studied takes place about 0.5 G above the position of the zero-energy resonance, the sensitivity of the pairwise projection technique decreases. This result coincides with the reported measurements of the condensed fraction of fermionic pairs extending up to about 0.5 G above the position of the zero-energy resonance.

VII. ACKNOWLEDGEMENTS

We are grateful to Paul Julienne, Peter Littlewood, Francesca Marchetti and Ben Simons for stimulating discussions. This research has been supported by Gonville and Caius College Cambridge (M.H.S.), the UK EPSRC (K.B.) and the Royal Society (K.G., T.K., and K.B.).

---

[1] L.V. Keldysh and You.V. Kopaev, *Fiz. Tverd. Tela* (Leningrad) **6**, 2791 (1964) [*Sov. Phys. Solid State* **6**, 2219 (1965)]; L.V. Keldysh and A.N. Kozlov, *Zh. Éksp. Teor. Fiz.* **54**, 978 (1968) [*Sov. Phys. JETP* **27**, 521 (1968)].

[2] D.M Eagles, Phys. Rev. **186**, 456 (1969).

[3] A.J. Leggett, in *Modern Trends in the Theory of Condensed Matter*, edited by A. Pekalski and R. Przystawa (Springer-Verlag, Berlin, 1980).

[4] P. Noziéres and S. Schmitt-Rink, J. Low Temp. Phys. **59**, 195 (1985).

[5] M. Randeria, in *Bose-Einstein Condensation*, edited by A. Griffin, D.W. Snoke, and S. Stringari (Cambridge University Press, Cambridge, 1995).

[6] M. Greiner, C.A. Regal, and D.S. Jin, Nature (London) **426**, 537 (2003).

[7] S. Jochim, M. Bartenstein, A. Altmeyer, G. Hendl, C. Chin, J. Hecker Denschlag, and R. Grimm, Science **302**, 2102 (2003).

[8] M.W. Zwierlein, C.A. Stan, C.H. Schunck, S.M.F. Raupach, S. Gupta, Z. Hadzibabic, and W. Ketterle, Phys. Rev. Lett. **91**, 250401 (2003).

[9] C.A. Regal, M. Greiner, and D.S. Jin, Phys. Rev. Lett. **92**, 040403 (2004).

[10] M.W. Zwierlein, C.A. Stan, C.H. Schunck, S.M.F. Raupach, A.J. Kerman, and W. Ketterle, Phys. Rev. Lett. **92**, 120403 (2004).

[11] M. Bartenstein, A. Altmeyer, S. Riedl, S. Jochim, C. Chin, J. Hecker Denschlag, and R. Grimm, Phys. Rev. Lett. **92**, 120401 (2004).

[12] T. Bourdel, L. Khaykovich, J Cubizolles, J. Zhang, F. Chevy, M. Teichmann, L. Tarruell, S.J.J.M.F. Kokkelmans, and C. Salomon, Phys. Rev. Lett. **93**, 050401 (2004).

[13] J. Kinast, S.L. Hemmer, M.E. Gehm, A. Turlapov, and J.E. Thomas, Phys. Rev. Lett. **92**, 150402 (2004).

[14] C. Chin, M. Bartenstein A. Altmeyer, S. Riedl, S. Jochim, J. Hecker Denschlag, and R. Grimm, Science **305**, 1128 (2004).

[15] M. Greiner, C.A. Regal, and D.S. Jin, Phys. Rev. Lett. **94**, 070403 (2005).

[16] M.W. Zwierlein, C.H. Schunck, C.A. Stan, S.M.F. Raupach, and W. Ketterle, Phys. Rev. Lett. **94**, 180401 (2005).

[17] M. Holland, S.J.J.M.F. Kokkelmans, M.L. Chiofalo, and R. Walser, Phys. Rev. Lett. **87**, 120406 (2001).

[18] E. Timmermans, K. Furuya, P.W. Milonni, and A.K. Kerman, Phys. Lett. A **285**, 228 (2001).

[19] J. Ranninger and S. Robaszkiewcz, Physica B **135**, 468 (1985).

[20] R. Friedberg and T.D. Lee, Phys. Rev. B **40**, 6745 (1989).

[21] T. Köhler, T. Gasenzer, and K. Burnett, Phys. Rev. A **67**, 013601 (2003).

[22] T. Köhler, T. Gasenzer, P.S. Julienne, and K. Burnett, Phys. Rev. Lett. **91**, 230401 (2003).

[23] J. R. Schrieffer, *Theory of Superconductivity* (Perseus Publishing, Cambridge, Massachusets, 1999).

[24] K. Góral, T. Köhler, S.A. Gardiner, E. Tiesinga, and P.S. Julienne, J. Phys. B **37**, 3457 (2004).

[25] K.E. Strecker, G.B. Partridge, and R.G. Hulet, Phys. Rev. Lett. **91**, 080406 (2003).

[26] T. Köhler, K. Góral, and T. Gasenzer, Phys. Rev. A **70**, 023613 (2004).

[27] S. Simonucci, P. Pieri, and G.C. Strinati, Europhys. Lett. **69**, 713 (2005).

[28] P.S. Julienne, private communication.

[29] P.B. Littlewood, P.R. Eastham, J.M.J. Keeling, F.M. Marchetti, B.D. Simons, and M.H. Szymańska, J. Phys.: Condens. Matter **16**, 3597 (2004).

[30] P. R. Eastham and P. B. Littlewood, Phys. Rev. B **64**, 235101 (2001).

[31] J. Keeling, P.R. Eastham, M.H. Szymańska, and P.B. Littlewood, Phys. Rev. Lett. **93**, 226403 (2004)

[32] G.M. Falco and H.T.C. Stoof, Phys. Rev. Lett. **92**, 130401 (2004).

[33] M. Mackie and J. Piilo, Phys. Rev. Lett. **94**, 060403 (2005).

[34] Given the background scattering length a_{bg}, the energy E_{-1} is determined solely by the van der Waals dispersion coefficient C_6 characterising the (non-retarded) asymptotic behaviour $V_{\mathrm{bg}}(r) \underset{r\to\infty}{\sim} -C_6/r^6$ of the exact microscopic background scattering potential at large inter-atomic distances r [cf. B. Gao, Phys. Rev. A **58**, 4222 (1998)].

[35] T. Loftus, C.A. Regal, C. Ticknor, J.L. Bohn, and D.S. Jin, Phys. Rev. Lett. **88**, 173201 (2002).

[36] P.S. Julienne and F.H. Mies, J. Opt. Soc. Am. B **6**, 2257 (1989).

[37] G.F. Gribakin and V.V. Flambaum, Phys. Rev. A **48**, 546 (1993).

[38] A. Derevianko , W.R. Johnson, M.S. Safronova , and J.F. Babb, Phys. Rev. Lett. **82**, 3589 (1999).

[39] M.H. Szymańska, K. Góral, and T. Köhler (unpublished).

[40] J. Fricke, Ann. Phys. (N.Y.) **252**, 479 (1996).

[41] T. Köhler and K. Burnett, Phys. Rev. A **65**, 033601 (2002).

[42] M.M. Parish, B. Mihaila, B.D. Simons, and P.B. Littlewood, Phys. Rev. Lett. **94**, 240402 (2005).

[43] Y. Ohashi and A Griffin, Phys. Rev. Lett. **89**, 130402 (2002).

[44] J.N. Milstein, S.J.J.M.F. Kokkelmans, and M.J. Holland, Phys. Rev. A **66**, 043604 (2002).

[45] A. Perali, P. Pieri, and G.C. Strinati, Phys. Rev. A **68**, 031601 (2003).

[46] R. Combescot, Phys. Rev. Lett. **91**, 120401 (2003).

[47] L. Viverit, S. Giorgini, L.P. Pitaevskii, and S. Stringari, Phys. Rev. A **69**, 013607 (2004).

[48] G.M. Bruun and C.J. Pethick, Phys. Rev. Lett. **92**, 140404 (2004).

[49] L.D. Carr, G.V. Shlyapnikov, and Y. Castin, Phys. Rev. Lett. **92**, 150404 (2004).

[50] T. Karpiuk, M. Brewczyk, and K. Rzążewski, Phys. Rev. A **69**, 043603 (2004).

[51] A. Perali, P. Pieri, L. Pisani, and G.C. Strinati, Phys. Rev. Lett. **92**, 220404 (2004).

[52] J. Stajic, J.N. Milstein, Q. Chen, M.L. Chiofalo, M.J. Holland, and K. Levin, Phys. Rev. A **69**, 063610 (2004).

[53] S. De Palo, M.L. Chiofalo, M.J. Holland, and S.J.J.M.F. Kokkelmans, Phys. Lett. A **327**, 490 (2004).

[54] H. Heiselberg, Phys. Rev. Lett. **93**, 040402 (2004).

[55] H.P. Büchler, P. Zoller, and W. Zwerger, Phys. Rev. Lett. **93**, 080401 (2004).

[56] A. Perali, P. Pieri, and G.C. Strinati, Phys. Rev. Lett. **93**, 100404 (2004).

[57] J. Kinnunen, M. Rodriguez, and P. Torma, Science **305**, 1131 (2004).

[58] J.E. Williams, N. Nygaard, and C.W. Clark, New J. Phys. **6**, 123 (2004).

[59] P.D. Drummond and K.V. Kheruntsyan, Phys. Rev. A **70**, 033609 (2004).

[60] A.V. Avdeenkov and J.L. Bohn, Phys. Rev. A **71**, 023609 (2005).

[61] M.M. Parish, B. Mihaila, E.M. Timmermans, K.B. Blagoev, and P.B. Littlewood, Phys. Rev. B **71**, 064513 (2005).

[62] A. Bulgac and G.F. Bertsch, cond-mat/0404301 (2004).

[63] R.B. Diener and T.-L. Ho, cond-mat/0404517 (2004).

[64] R.B. Diener and T.-L. Ho, cond-mat/0405174 (2004).

[65] L.M. Jensen, cond-mat/0412431 (2004).

[66] J.W. Negele and H. Orland, *Quantum many-particle systems* (Perseus, Cambridge, Massachusetts, 1998).

[67] K. Góral and K. Burnett, Phys. World **17** (3), 23 (2004).